Archaeomagnetic and rock magnetic study of six kilns from North Africa (Tunisia and Morocco)

Miriam Gomez Paccard, Greg Mcintosh, Annick Chauvin, Elisabet Beamud, Francisco J. Pavon-Carrasco, Jacques Thiriot

Geophysical Journal International

Geophys. J. Int. (2012) **189,** 169–186 doi: 10.1111/j.1365-246X.2011.05335.x

Archaeomagnetic and rock magnetic study of six kilns from North Africa (Tunisia and Morocco)

Miriam Gómez-Paccard,[1] Gregg McIntosh,[2,3] Annick Chauvin,[4] Elisabet Beamud,[5] Francisco J. Pavón-Carrasco[3] and Jacques Thiriot[6]

[1] *Institut de Ciències de la Terra Jaume Almera, ICTJA-CSIC, Lluís Solé i Sabarís s/n,* 08028 *Barcelona, Spain. E-mail: mgomezpaccard@ictja.csic.es*
[2] *Instituto de Geociencias (UCM-CSIC), Facultad de Ciencias Físicas, Universidad Complutense de Madrid, Avda Complutense s/n,* 28040 *Madrid, Spain*
[3] *Departamento de Física de la Tierra, Astronomía y Astrofisica I (Geofísica y Meteorologia), Facultad de Ciencias Físicas, Universidad Complutense de Madrid, Avda Complutense s/n,* 28040 *Madrid, Spain*
[4] *Géosciences-Rennes, CNRS, UMR* 6118, *Université de Rennes 1, Campus de Beaulieu,* 35042 *Rennes, Cedex, France*
[5] *Grup de Geodinàmica i Anàlisi de Conques (GGAC), GEOMODELS Research Institute, Laboratori de Paleomagnetisme CCiTUB-CSIC, Institut de Ciències de la Terra Jaume Almera, CSIC, Solé i Sabarís s/n,* 08028 *Barcelona, Spain*
[6] *Laboratoire d'archéologie médiévale méditerranéenne, UMR* 6572, *Maison méditerranéenne de Sciences de l'Homme, CNRS,* 13094 *Aix-en-Provence, France*

Accepted 2011 December 12. Received 2011 October 18; in original form 2011 July 15

SUMMARY

New full-vector archaeomagnetic data for North Africa recovered from the study of six kilns, five from Tunisia and one from Morocco, are presented. Archaeological and historical considerations, along with three radiocarbon dates, indicate that the age of the kilns ranges between the 9th and 15th centuries AD. Rock magnetic analyses showed that the principal magnetic carriers are magnetite and low Ti titanomagnetite, along with variable contributions of thermally stable maghemite and a high coercivity phase with low unblocking temperatures. The magnetic mineralogy of the studied material is thermally stable and behaves ideally during archaeointensity experiments. Stepwise alternating field demagnetization isolated a single, stable, characteristic remanence component with very well defined directions at both specimen and structure levels. Mean archaeointensities have been obtained from successful classical Thellier experiments conducted on between five and eight independent samples per kiln. Thermoremanent magnetization (TRM) anisotropy and cooling rate effects upon TRM intensity have been investigated. The results showed that these effects are low for four of the six studied kilns, with differences between the uncorrected and corrected means of less than 3 per cent. For the other two structures differences between the uncorrected and corrected mean site intensities are 4.4 per cent and 5.8 per cent. These results highlight the necessity for TRM anisotropy and cooling rate corrections in archaeomagnetic studies if accurate archaeointensities are to be obtained. The new results suggest that high intensities occurred in Northwest Africa during the 9th century. Although more data are clearly needed to define this period of high intensity, the results are in agreement with the available European archaeointensity data. A comparison between the new data, other available archaeomagnetic determinations in nearby locations, and palaeosecular variation (PSV) curves derived from the regional SCHA.DIF.3k and global ARCH3K.1 geomagnetic field models shows good agreement between the new data and directional results derived from the models. However, some differences are observed between geomagnetic field models intensity results and available archaeointensity data for the studied regions. This highlights the need for new data for unexplored regions such as North Africa. The new data presented here better constrains the evolution of the geomagnetic field during historical times in this region. They represent a new step towards the construction of a reference PSV curve for Northwest Africa. Once established, this curve will represent a new dating method for this region.

Key words: Archaeomagnetism; Palaeointensity; Palaeomagnetic secular variation; Rock and mineral magnetism; Africa.

1 INTRODUCTION

Archaeomagnetic data are used to compute regional palaeosecular variation (PSV) curves (e.g. Schnepp & Lanos 2005; Gómez-Paccard *et al*. 2006b, 2008; Tema *et al*. 2006; Márton 2010) or regional/global geomagnetic field models (e.g. Korte *et al*. 2009; Pavón-Carrasco *et al*. 2009) that can help to describe the temporal and the spatial behaviour of the geomagnetic field on a centennial/millennial scale. Obviously, the accuracy and the validity of such regional curves and models rely on the quality, the quantity and the spatial and time distribution of the data used for their construction. Future progress in geomagnetic research is therefore dependent on the availability of new, reliable and well-dated data from unexplored regions.

Up to now, very few data are available for Northwest Africa (Fig. 1). For Morocco there are seven directional data (Kovacheva 1984; Najid 1986) and four archaeointensity data (Kovacheva 1984; Casas *et al*. 2008) for the last two millennia (Supporting Information). For Tunisia one directional and two intensity data have been published for the first millennium BC (Thellier & Thellier 1959), but no archaeomagnetic data are available for the last 2000 years. The study of Odah *et al.* (1995) includes one intensity data from a site in Libya that is close to the Tunisian border.

This research addresses this shortfall by presenting new archaeomagnetic results from three archaeological sites in Northwest Africa (Fig. 1): Sabra al-Mansuriya, Raqqada (Tunisia) and Rirha (Morocco). The new full-vector information is a start in filling the gap for this region and may be extremely useful for future constructions of PSV curves and geomagnetic field models. Once established, these curves and models will represent a new dating tool for burned archaeological remains from this region.

2 ARCHAEOLOGICAL CONTEXT AND DATING

Six very well preserved kilns have been studied. Five of them come from two archaeological sites in Tunisia, North Africa: a brick-firing kiln (RQD-105, Fig. 2a) from Raqqada, 9 km south of Kairouan and three pottery-firing kilns (SBR-6038, SBR-6043 and SBR-6081, Fig. 2b–d) and a glass-firing kiln (SBR-FV, Fig. 2e) from Sabra al-Mansuriya, now part of urban Kairouan (Fig. 1). Raqqada was the capital of the Aghlabid dynasty, which controlled an area encompassing eastern Algeria, Tunisia and parts of modern day Libya during the 9th century AD. The city may have been occupied by the Aghlabids from the beginning of the 8th century AD and fell to the Fatimid dynasty in 909 AD. It was abandoned in the first quarter of the 10th century AD when the Fatimids moved to the new capital Mahdiya. Sabra al-Mansuriya was founded a little later, in 947–948 AD, marking the return of caliphate power in the region around Kairouan. It remained the capital of the Zirid governors up to 975 AD when the caliphate leader was installed in Cairo. Bedouin tribes eventually overthrew the Zirids, and Kairouan was abandoned around the middle of the 11th century AD.

In Raqqada the last period of use of kiln RQD-105 was before the construction of the Dar al-Bahr Palace in 905 AD. Two radiocarbon dates obtained from charcoal samples studied at the Centre de datation pour le Radiocarbone (CNRS, Université Claude Bernard Lyon 1) are also available. The first radiocarbon sample was taken from RQD-105 and places its use between 673 and 857 calibrated years AD, at a 95 per cent confidence level. The second radiocarbon sample corresponds to a different structure that was in use after RQD-105 and gives an age of 782–976 calibrated years AD at a 95 per cent confidence level. This latter age is in agreement with archaeological and historical evidence that place the abandonment of Raqqada at 905 AD. Together, the historical/archaeological constraints and radiocarbon dates place the last use of the kiln RQD-105 between 800 and 905 years AD.

For the kilns sampled at Sabra al-Mansuriya, archaeological and stratigraphic constraints indicate that kilns SBR-6038 and SBR-6043 were abandoned before kilns SBR-6081 and SBR-FV. The earliest use of the kilns could coincide with the founding of the city in 947–948 AD, although it is more likely that the workshop was established some time after the caliphate moved to Cairo in 975 AD (Cressier, personal communication, 2011). The abandonment of the ceramic and glass workshop appears to be contemporaneous with the capture and destruction of the city in 1057 AD (Cressier & Rammah 2004, 2006; Thiriot 2009). On this basis the last use of the kilns has been placed between 1000 and 1057 AD.

One kiln (RHA) from Rirha (Garb region), Morocco, has been studied (Figs 1 and 2f). Rirha is located 35 km northwest of the archaeological site of Volubilis and 8 km north of Sidi Slimane (Kénitra province). Rirha is a city dating back to the Mauritanian and Roman periods. Archaeological remains found in this site include mosaics, burial inscriptions, pottery and coins. Three phases of occupation can be distinguished: the Mauritanian phase dating back to the 5th century BC, the Roman occupation of the site between the 1st and the 3rd centuries AD and the Islamic phase between the 9th and the 14–15th centuries AD. Kiln RHA corresponds to the Islamic occupation and has been dated by archaeological constraints and one radiocarbon date performed at the Poznan Radiocarbon laboratory (Callegarin *et al*. 2006, 2011; Coll-Conesa *et al*. 2011). The radiocarbon (charcoal) sample gave an age between 1290 and 1410 calibrated years AD at a 95 per cent confidence level. Therefore the last use of the kiln has been placed inside this interval. The ages ascribed to each one of the kilns studied for archaeomagnetism are shown in Table 1.

3 METHODOLOGY

3.1 Sampling

At least 18 independently oriented block samples were taken from each kiln. The samples were composed of well-consolidated burned clay or bricks and were oriented by magnetic and solar compass on a horizontal surface prepared using plaster of Paris (Figs 2a–f). The block samples were then subsampled at the Palaeomagnetism Laboratory of the Universidad Complutense (Madrid, Spain) by cutting cubic specimens (2 cm side) close to the interior (most heated) faces of each block. To retrieve the archaeomagnetic directions one specimen per sample was used. Between six and 10 unoriented cubes, one per sample, were used for the archaeointensity experiments.

3.2 Laboratory treatment

The archaeodirectional study was carried out in the Palaeomagnetism Laboratory of the Universidad Complutense (Madrid, Spain). Alternating field (AF) demagnetization of the natural remanent magnetization (NRM) was carried out using a 755–4K SRM (2G Enterprises) superconducting rock magnetometer with an in-line AF demagnetiser or a JR-5 (AGICO) spinner magnetometer and a GSD-5 (Schonsted) AF demagnetizer. AF demagnetization

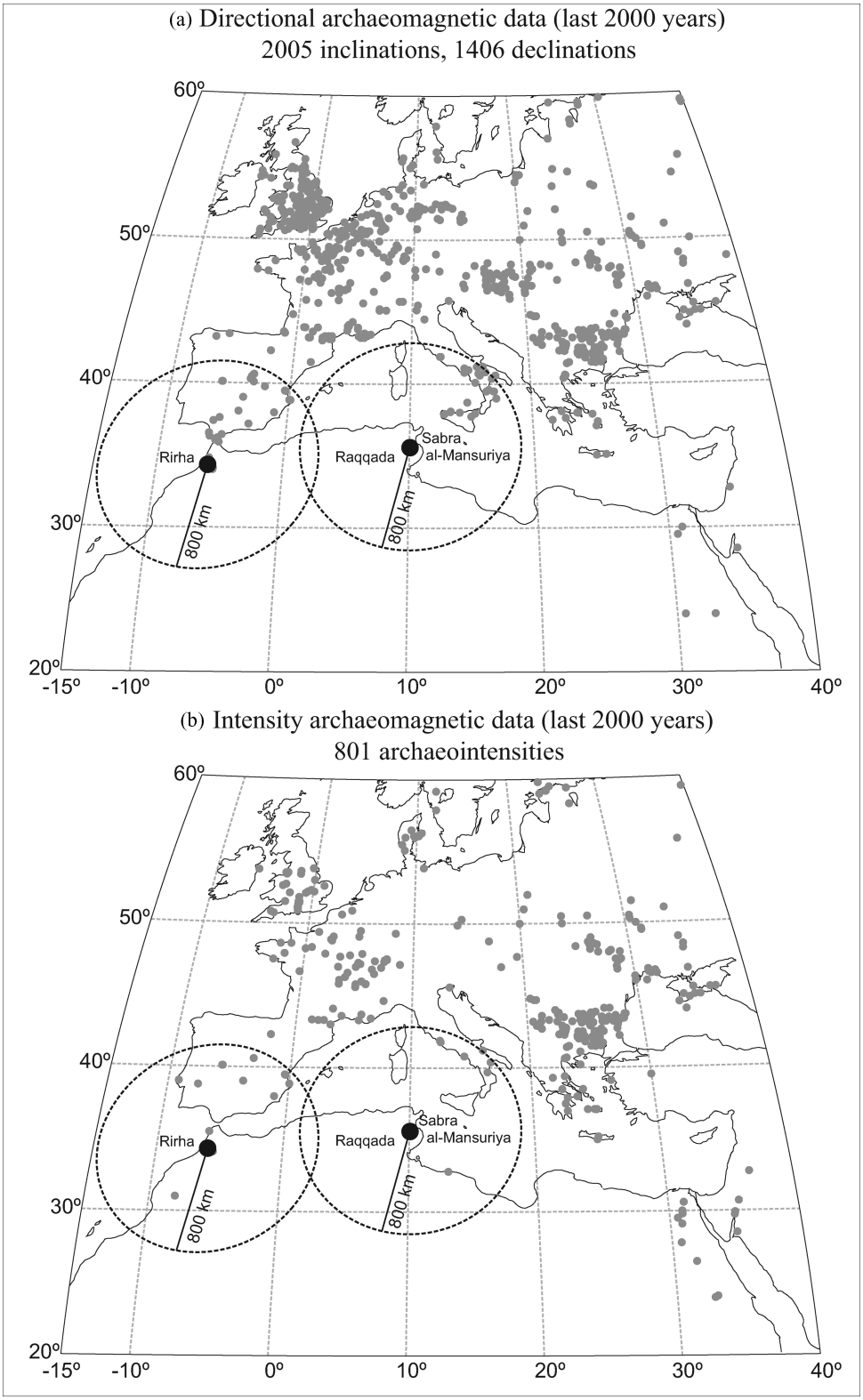

Figure 1. Map of Europe and North Africa showing the location of Rirha, Sabra al-Mansuriya and Raqqada (black dots). Grey circles indicate location of other directional available directional (a) or archaeointensity (b) data.

was carried out with at least seven steps up to a maximum peak AF of 100–120 mT.

Archaeointensity experiments were carried out at the Palaeomagnetism Laboratories of the Institute of Earth Sciences Jaume Almera (Barcelona, Spain) and Géosciences-Rennes (Rennes, France), following the classical Thellier palaeointensity method (Thellier & Thellier 1959). This method is based on the comparison of the NRM lost and the partial thermoremanent magnetization (pTRM)

Figure 2. Photographs of the sampled kilns at (a) Raqqada, (b)–(e) Sabra al-Mansuriya and (f) Rirha.

gained in a known laboratory field at progressively higher temperatures. Remanent magnetization was measured on a 755R SRM (2G Enterprises) superconducting rock magnetometer. Specimens were heated in a MMTD-80 (Magnetic Measurements) furnace from 100°C up to temperatures at which more than 85 per cent of the initial magnetization was lost. A laboratory field of 50 μT was applied. At each temperature step, samples were first heated and cooled with the laboratory field applied along their *Z*-axis and second, were heated and cooled with the laboratory field applied in the opposite sense. Between seven and 19 temperature steps were needed. The TRM anisotropy tensor was calculated for each specimen from TRM acquisition in six different directions. The cooling rate dependence of TRM intensity was also analysed by measuring four additional TRM acquisition steps at the end of the Thellier experiments. Comparing the rapid (the typical laboratory cooling time of about 1.5 hours) and slow cooling results (about 24 hours) allowed the quantification of the cooling rate effect upon archaeointensity estimates for each specimen. For a detailed description of the experimental procedures followed in the archaeointensity protocol see Gómez-Paccard *et al.* (2006a).

Rock magnetic studies were carried out on AF demagnetized specimens or on subsamples prepared from block off-cuts at the Palaeomagnetism Laboratory of the Complutense University (Madrid). Low field magnetic susceptibility (κ) of each archaeodirectional specimen was measured using a KLY-3 kappabridge (AGICO). Magnetic hysteresis and backfield isothermal remanence (IRM) curves were measured on crushed samples using a J-Meter coercivity meter (Iassanov *et al.* 1998) with a maximum applied field of 500 mT. Backfield IRM curves were measured on additional AF demagnetized specimens using a JR-5 (AGICO) spinner magnetometer and an IM-10–30 (ASC Scientific) impulse magnetizer with a maximum applied field of 2 T. The same specimens were used to study the thermal (TH) demagnetization of orthogonal IRMs (Lowrie 1990), separating the total IRM into soft (0–0.1 T), medium (0.1–0.3 T) and hard (0.3–2 T) components. The specimens were demagnetized using a TSD-1 (Schonsted) thermal demagnetizer. Strong field thermomagnetic curves (in air, heating rate 40°C min^{-1}, applied field 300 mT) of representative crushed subspecimens were measured using a MMVFTB (Petersen Instruments) variable field translation balance.

4 MAGNETIC MINERALOGY

Initial NRM intensities and κ of the archaeodirectional specimens ranged over several orders of magnitude, with the highest values observed for the RHA (Morocco) specimens (Fig. 3). Koenigsberger ratios (defined as $Q_n = \mathrm{NRM}/\kappa H$, with $H = 39$ A m^{-1}) between 5 and 30 are consistent with a thermomagnetic origin for the NRM.

In total, 45 magnetic hysteresis experiments have been performed. All but four yielded magnetic hysteresis curves that showed reversible behaviour by 300 mT and backfield IRM curves that reached saturation by 300 mT (e.g. sample SBR-6081–08, Fig. 4a). Therefore the increase in magnetization between 300 and 500 mT is considered to be due to paramagnetic behaviour, whose contribution has been estimated from the slope of the descending branch of hysteresis curve between 500 and 300 mT. Four samples exhibited curves that were slightly non-reversible beyond 300 mT and backfield IRM curves that did not approach saturation (e.g. RQD-105–06, Fig. 4b). This high field behaviour has been considered as

Table 1. Location of the archaeomagnetic sites and a summary of the information used to date the different kilns.

Site	Latitude (°)	Longitude (°)	Kiln	Dating method	Dating (yr AD)
Raqqada	35.60 N	10.06 E	RQD-105	Historical/archaeological constraints + radiocarbon dates	800–905
Sabra al-Mansuriya	35.66 N	10.10 E	SBR-FV	Historical/archaeological constraints	1000–1057
			SBR-6038	Stratigraphic constraints indicate that 6038	1000–1057
			SBR-6043	and 6043 were abandoned before 6081 and FV	1000–1057
			SBR-6081		1000–1057
Rirha	34.31 N	5.93 W	RHA	Archaeological constraints + radiocarbon date	1290–1410

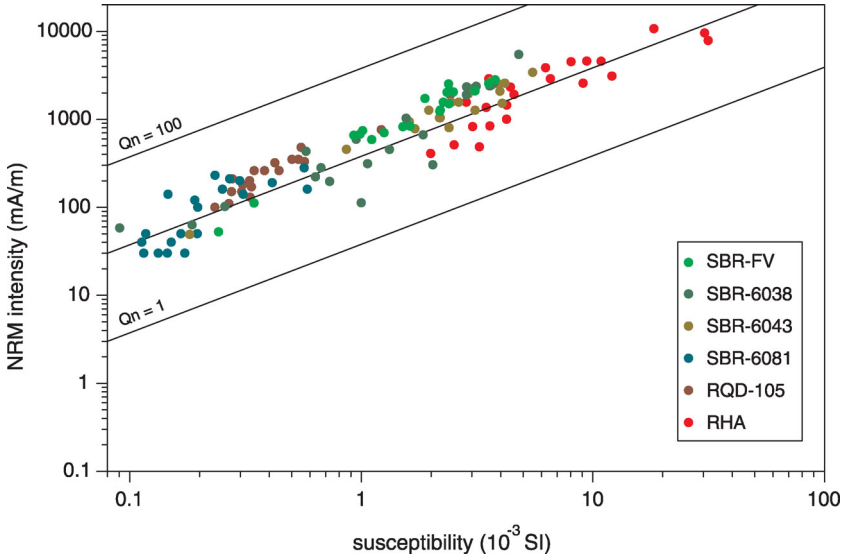

Figure 3. Intensity of the natural remanent magnetization (NRM) versus bulk susceptibility. Lines indicate constant Koenigsberger (Q_n) values.

a mixture of paramagnetic and unsaturated ferromagnetic (*s.l.*) contributions. For these samples the high-field contribution has been calculated from the descending branch of the curve between 500 and 450 mT.

After high-field correction, saturation magnetization (M_s) varied between 0.51 and 371 $mAm^2\ kg^{-1}$ and coercive force (B_c) between 3 and 25 mT. The highest values of M_s and saturation remanence (M_{rs}) were observed for samples from kiln RHA (Morocco).

The vast majority of backfield IRM curves (37 of 45) were square-shaped, showing a sharp change in IRM below 200 mT and minor amounts of high-coercivity IRM beyond 300 mT (SBR-6038–19 and SBR-6043–02, Fig. 4c), with coercivity of remanence (B_{cr}) values ranging between 12 and 59 mT. A further eight samples exhibited a greater proportion of high coercivity IRM, with the shape of the curve clearly suggesting the presence of distinct coercivity phases (SBR-FV-04, Fig. 4c) of varying contributions. This included six samples from structure RQD-105 and two from structure SBR-FV. B_{cr} values ranged between 29 and 233 mT, H_{cr} increasing as the proportion of IRM acquired above 300 mT increases.

When plotted together on a Day plot (Day *et al*. 1977; Fig. 4d), the results tend to group together within the pseudo-single domain region. Six outlying values plot to the right of the main group, showing relatively high B_{cr}/B_c ratios. This includes four samples from structures RQD-105 and SBR-FV, which acquired a large proportion of IRM beyond 300 mT and thus exhibit relatively high H_{cr} values. The other two samples are from kiln SBR-6043. They differ from the RQD-105 and SBR-FV samples in that they show a relatively small amount of IRM acquisition beyond 300 mT. They do have small B_c values (4 and 6 mT), which may contribute to the high B_{cr}/B_c values.

Thermal demagnetization of orthogonal IRMs indicated that the soft (0–0.1 T) IRM component dominated the total IRM in nine of the 10 studied samples, in all cases exhibiting maximum unblocking temperatures of 540–620 °C (e.g. RHA-17, Fig. 4e). In the case of sample RQD-105–07 (Fig. 4f) the soft (0–0.1 T) and hard (0.3–2 T) components contributed almost equally to the total IRM. The hard component was dominated by demagnetization between 100 and 200°C (Fig. 4f). This was a thermally stable feature, with the same IRM and unblocking temperatures observed when repeating the acquisition and demagnetization after heating to 700°C (green symbol, Fig. 4f). Similar unblocking temperatures and thermal stabilities were observed for the hard (0.3–2 T) component of the other two RQD-105 samples studied, although it contributed less to the total IRM. The hard component demagnetization curves of the remaining samples were noisy, although maximum unblocking temperatures of around 620–700°C could be tentatively identified in four cases.

Twelve thermomagnetic curves have also been measured. The results showed a high degree of reversibility, indicating that no important magnetomineralogical changes occurred during heating. Five of the curves showed a single change in slope on the heating and cooling curves (e.g. RHA-22, Fig. 4g), which suggests a single dominant ferromagnetic phase. Curie temperatures (T_c) were calculated using the second derivative of the heating curve (Tauxe 1998), yielding values of 575–628°C. Five samples showed a second, poorly expressed slope change (e.g. SBR-6081–20, Fig. 4h), indicating the presence of two ferromagnetic phases with T_cs of 214–460°C and 560–589°C. The remaining two curves did not show a discernible slope change and no reliable T_c could be calculated.

Together, the results suggest that the magnetic mineralogy of the studied material is thermally stable and thus well suited to archaeomagnetic and archaeointensity studies. The kilns SBR-6038, SBR-6043 and SBR-6081 (Sabra al-Mansuriya) and RHA (Rirha) are dominated by low coercivity magnetic phases ($H_c \leq 25$ mT and $H_{cr} \leq 59$ mT). T_cs of 560–602°C support the presence of magnetite or low titanium titanomagnetite, along with some maghemite that may be giving rise to the slightly elevated T_cs. Samples from kilns SBR-6043 and SBR-6081 also show T_cs of 330–460°C, which can be explained by the presence of titanomagnetite with higher titanium content. Similar unblocking temperatures of both IRM and NRM confirm that they contribute to the stable remanence of the material. Kilns SBR-FV (Sabra al-Mansuriya) and RQD-105 (Raqqada) also show a low coercivity phase, with T_cs of 575–628°C and unblocking temperatures (IRM and NRM) of 570–630°C supporting the presence of magnetite and/or maghemite.

Samples from Sabra (SBR-FV) and Raqqada (RQD-105), both near Kairouan, show the variable presence of a high coercivity phase with remanence coercivities greater than 0.3 T, IRM unblocking

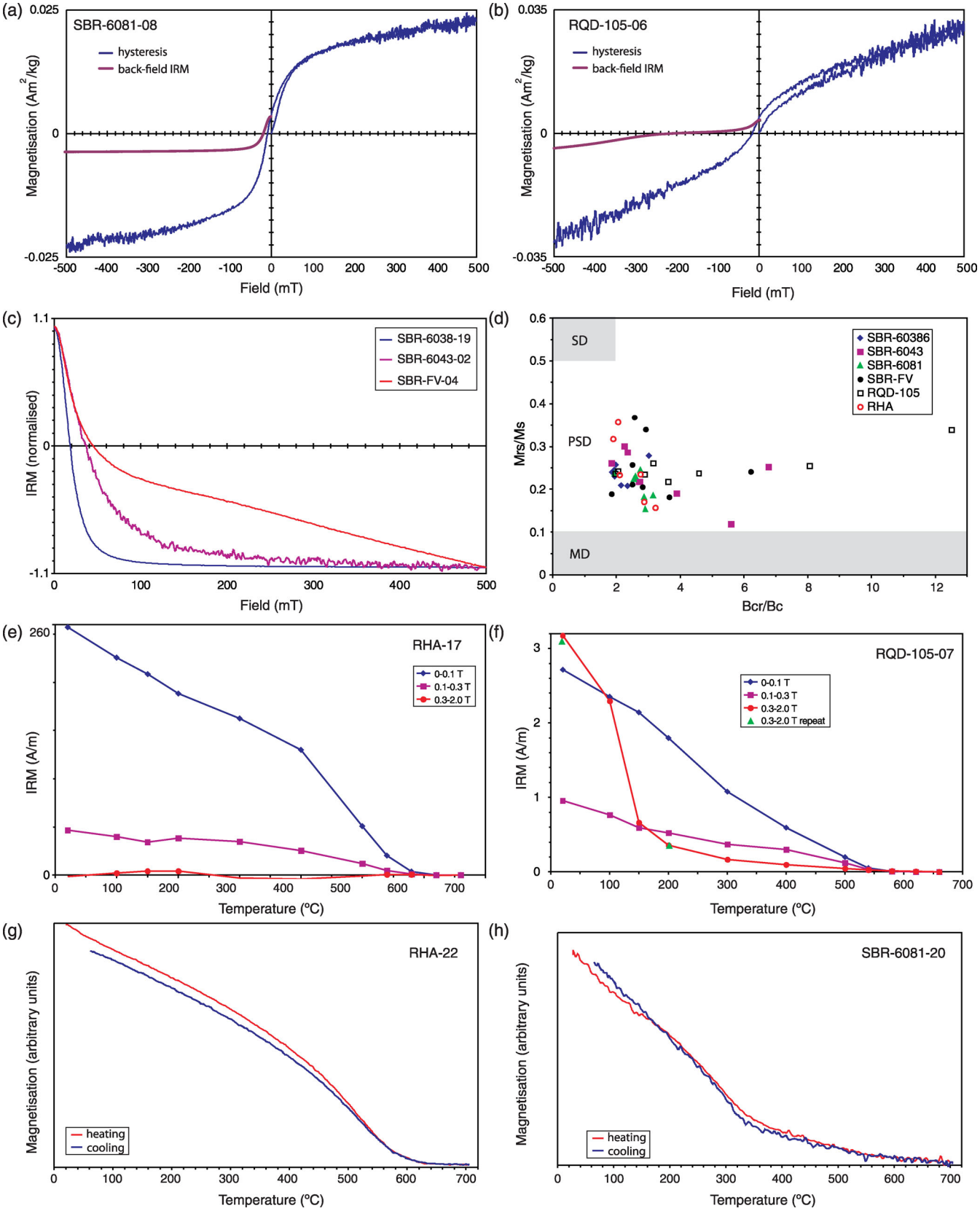

Figure 4. Representative rock magnetic results. (a)–(b) Hysteresis curves, (c) backfield isothermal remanence (IRM) curves, (d) Day plot of magnetization and coercivity ratios, (e)–(f) thermal demagnetization of IRM and (g)–(h) strong field thermomagnetic curves.

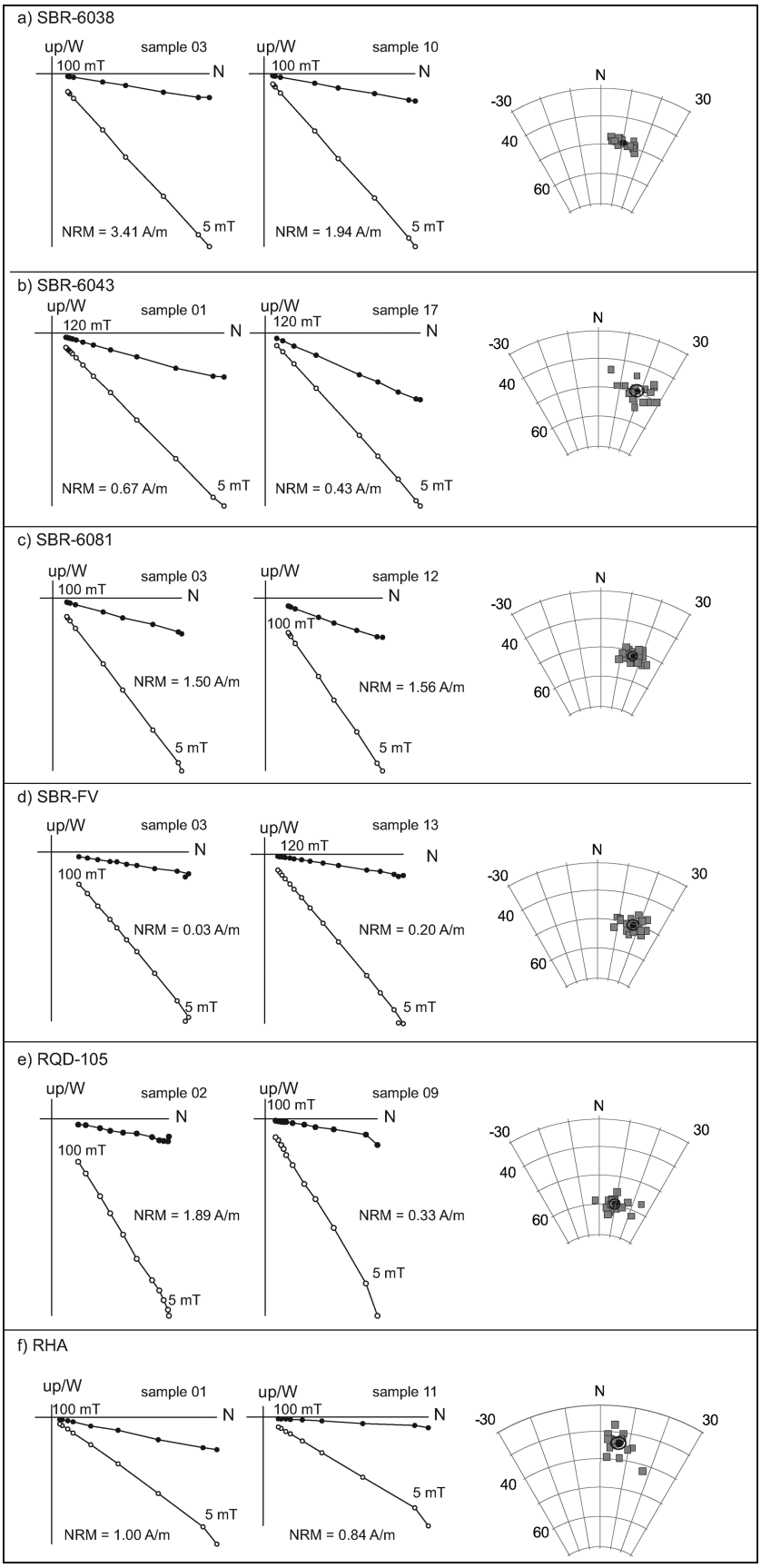

Figure 5. Directional results. The left-hand side shows two representative orthogonal vector plots of AF demagnetization of NRM, with solid/open symbols denoting projection on the horizontal/vertical plane. The right hand side shows stereoplots of specimen characteristic directions in grey and the mean direction and α_{95} in black.

Table 2. Summary of archaeomagnetic directions obtained from AF demagnetization. Site, archaeological site where the kiln was sampled; Kiln, name of the kiln; Age, age of the structure in yr AD; n, number of samples taken into account for the calculation of mean directions; D_s, I_s, mean declination and inclination *in situ*; α_{95}, 95 per cent confidence cone of mean directions and k, precision parameter (Fisher 1953).

Site	Kiln	Age (yr AD)	n	D_s (°)	I_s (°)	α_{95} (°)	k
Raqqada	RQD-105	800–905	19	9.8	59.7	1.5	495.3
Sabra al-Mansuriya	SBR-FV	1000–1057	20	15.0	50.7	1.5	503.0
	SBR-6038	1000–1057	18	11.3	49.0	1.2	841.2
	SBR-6043	1000–1057	18	17.7	49.4	2.1	261.6
	SBR-6081	1000–1057	19	16.7	52.3	1.3	710.8
Rirha	RHA	1290–1410	18	6.8	33.6	1.9	328.2

temperatures of 100–300°C and T_cs of around 230°C. This phase is particularly common in samples from kiln RQD-105 where it may contribute more than half of the total IRM. NRM unblocking temperatures around 150–300°C and AF coercivities in excess of 100 mT suggest that the same phase contributes to the stable remanence of the material.

This phase shares the same characteristics as those exhibited by a thermally stable, high coercivity and low unblocking temperature phase described by McIntosh *et al.* (2007, 2011). They ascribe the phase to either hemoilmenite, inherited by the baked clays from adequate source rocks, or to substituted hematite or iron cristobalite, formed through the transformation of iron-rich clays during heating. The geology of the catchment area surrounding Kairouan consists of Tertiary and Quaternary sediments overlying Cretaceous limestones and marls (Dassi *et al*. 2005). Although Neogene volcanism is predominantly restricted to more northerly areas of Tunisia (e.g. Maury *et al*. 2000), the presence of titanomagnetite in kilns SBR-6043 and SBR-6081 would suggest that some volcanic-derived sediments are available around Kairouan that may also provide a viable hemoilmenite source. Differentiating between inherited hemoilmentite and neoformed hematites or iron cristobalite is not possible without more detailed knowledge of sediment sources, further magnetic tests (such as those summarized by McIntosh *et al.* (2011)), and/or microscopy studies.

There was some evidence for the presence of hematite in the IRM results that showed poorly defined unblocking temperatures of up to 650–700°C, although its contribution to the magnetic properties was minor in all cases. Where samples showed a large high coercivity contribution, this was always associated with unblocking temperatures lower than 300°C.

5 NEW ARCHAEOMAGNETIC RESULTS FOR NORTHWEST AFRICA

5.1 Characteristic directions

Progressive AF demagnetization revealed a single, stable NRM component between 5–10 mT and 100 or 120 mT (Figs 5a–f) in all but three of the specimens analysed. In most cases at least 85 per cent of NRM was demagnetized by 100–120 mT, although in isolated cases up to 58 per cent of NRM remained. This high coercivity NRM always preserved the same direction as the low coercivity NRM, suggesting that it represents the same stable NRM component, which is likely the TRM acquired during the last use of the kilns. Specimens from kilns SBR-FV (Fig. 5d) and RQD-105 (Fig. 5e) tended to have higher proportions of AF-resistant NRM.

Principal component analysis (Kirschvink 1980) was used to calculate the best-fit direction of the characteristic magnetization,

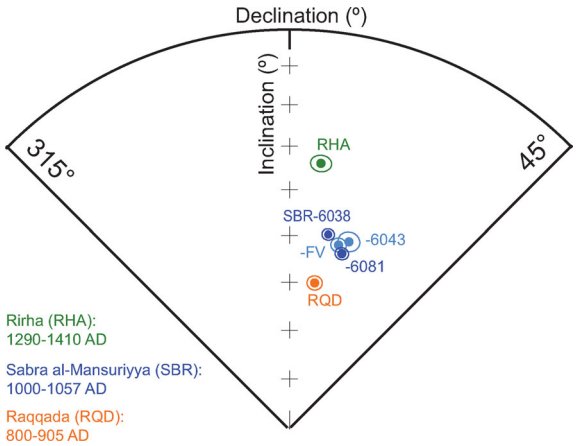

Figure 6. Stereographic projection of the mean direction of magnetization with α_{95} error circles of the new African data. All data relocated to Sabra al-Mansurinya.

yielding well-defined directions with maximum angular deviations (MAD) of less than 2°. The mean directions obtained for each kiln were calculated using Fisher (1953) statistics. The resulting means are very well defined, with their associated confidence angles (α_{95}) lower than 1.5° for all the structures except for SBR-6043 and RHA, which have α_{95} of 2.1° and 1.9°, respectively (Table 2 and Fig. 5). Fig. 6 shows equal area projections of site mean directions. Similar directions were obtained for kilns SBR-FV, SBR-6038, SBR-6043 and SBR-6081which, taking into account the errors, is in agreement with the available archaeological/historical information that proposed the same age interval for these structures (Table 1). The results do not distinguish the relative age difference between the kilns that was provided by their stratigraphic relationship. The mean site directions obtained indicate that important changes in inclination (of ∼30°) occurred in North Africa between the 9th and the 15th centuries (Fig. 6). This illustrates the potential of PSV geomagnetic field changes as a dating tool in Northwest Africa.

5.2 Archaeointensity determination

Archaeointensity estimations were attempted on 48 specimens, between 6 and 10 per structure. As rock magnetic experiments suggested, the magnetic carriers were stable during Thellier experiments. Very high quality linear NRM-TRM diagrams with successful pTRM checks were obtained corresponding to well-defined single component magnetizations trending toward the origin (Figs 7a–f). Maximum unblocking temperatures between 430–460°C (Fig. 7c) and 630°C (Fig. 7e) were obtained, in broad

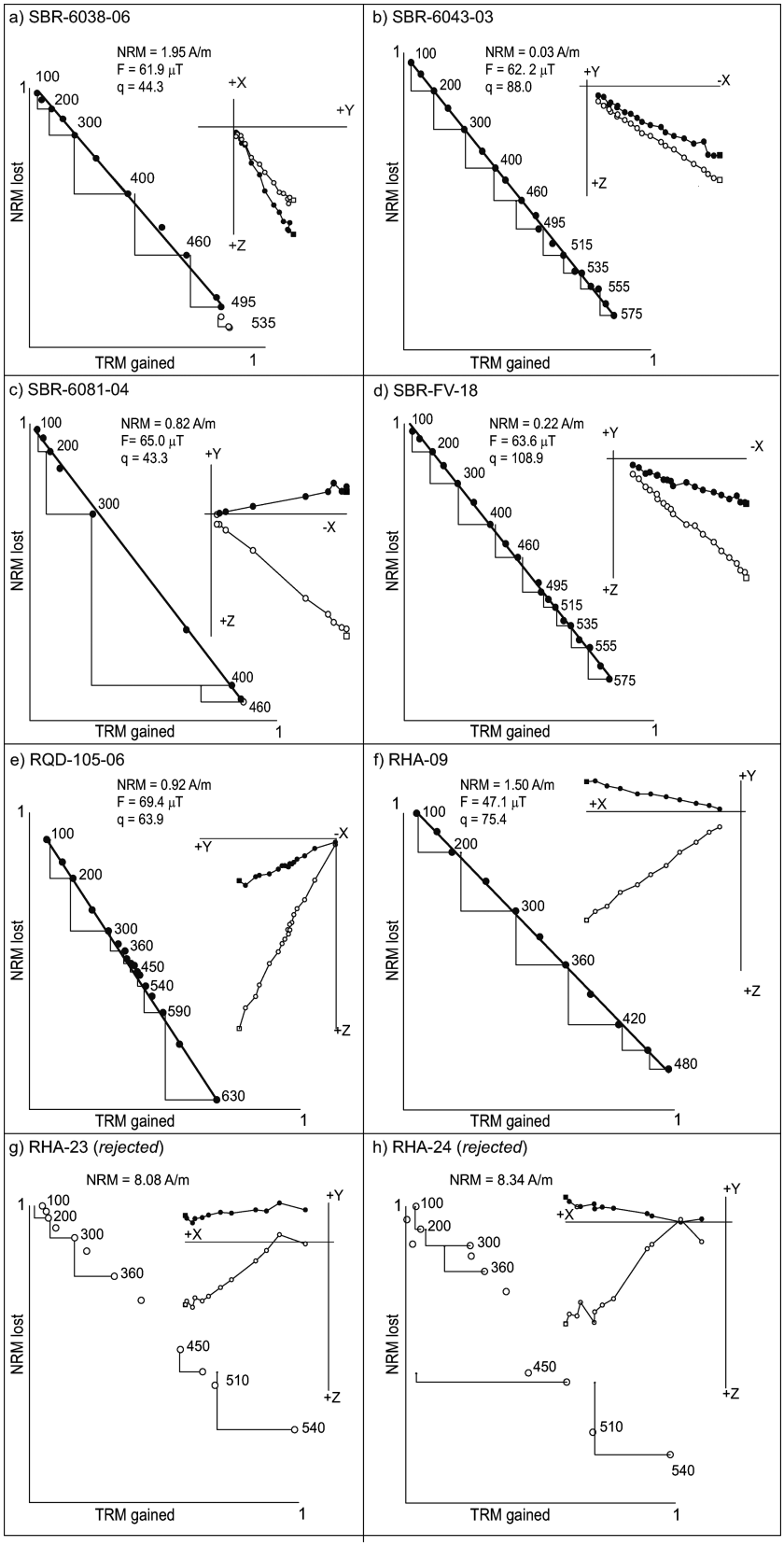

Figure 7. Archaeointensity results. Typical Arai plots of NRM lost against TRM gained. Solid symbols indicate data used for archaeointensity determinations. The initial NRM values, the intensity (F) and quality factor (q) obtained for each specimens are indicated. Temperatures are in °C. Also shown are the orthogonal vector projections of the NRM in sample coordinates, with solid/open symbols denoting projection on the horizontal/vertical plane.

Table 3. Summary of archaeointensity results. Kiln, name of the kiln; Sp., sample number; NRM, intensity of the natural remanent magnetization in A m^{-1}; κ, initial susceptibility in 10^{-6} SI units; $T_{min} - T_{max}$, temperature interval used for the slope calculation in °C; n, number of data points within this temperature interval; f, fraction of the NRM component used in the slope calculation; g, gap factor; q, quality factor; MAD, maximum angle of deviation; DANG, deviation angle; CRM, potential error on the estimation of the palaeointensity due to the acquisition of CRM as a percentage of the applied field; $F \pm \sigma F$, intensity estimate and its standard error per specimen without TRM anisotropy correction; Fe, intensity estimate per specimen after correction of TRM anisotropy; Fm ± s.d., TRM anisotropy corrected mean intensity per site and standard deviation; Fpo, weighted mean intensity per site; ΔTRM (24 hr), correction factor per sample for a cooling time of about 24 hr; alt (24 hr), alteration factor per sample for a cooling time of about 24 hr; Fpocr, weighted mean intensity per site after TRM anisotropy and cooling rate corrections; VDM and VADM, value of the virtual dipole moment and virtual axial dipole moment, respectively.

Kiln	Sp.	NRM (A m^{-1})	κ (10^{-6})	$T_{min} - T_{max}$ (°C)	n	f	g	q	MAD (°)	DANG (°)	CRM (per cent)	$F \pm \sigma F$ (μT)	F_e (μT)	Fm ± sd (μT)	Fpo (μT)	ΔTRM (24 hr) (per cent)	alt. (24 hr) (per cent)	Fpocr (μT)	VDM 10^{22} A m^2	VADM 10^{22} A m^2
RQD-105	02	1.89	2286	100–630	17	0.95	0.86	24.3	1.7	1.3	6.6	77.0 ± 2.6	55.5	66.6 ± 6.8	67.4	4.0	1.7	65.6± 6.2	11.3	11.9
(800–905 AD)	04	0.30	688	100–590	15	0.79	0.86	40.9	1.0	0.2	2.8	75.9 ± 1.3	75.7			7.7	1.3			
	06	0.92	864	100–630	17	0.87	0.90	63.9	2.8	1.3	7.1	69.4 ± 0.8	70.7				>ΔTRM			
	08	0.21	344	100–540	13	0.78	0.86	41.1	0.9	0.1	2.7	70.3 ± 1.2	70.7			4.0	0.0			
	10	0.23	334	100–540	13	0.83	0.86	50.1	1.0	0.3	3.1	63.0 ± 0.9	62.7				>ΔTRM			
	12	0.22	322	100–540	13	0.82	0.86	86.9	1.6	0.3	3.8	66.8 ± 0.5	66.1			1.8	–0.8			
	14	0.33	390	100–540	13	0.82	0.85	30.8	1.2	0.9	2.5	59.5 ± 1.3	59.8			3.0	–0.9			
	20	0.19	266	100–540	13	0.73	0.88	45.5	2.5	0.2	7.0	72.1 ± 1.0	71.8			3.7	–0.9			
SBR-FV	03	0.05	160	100–430	8	0.54	0.78	12.1	3.5	2.2	5.7	46.1 ± 1.6	46.2	63.1 ± 10.8	64.2	12.6	2.7	62.8 ± 12.7	12.1	11.4
(1000–1057 AD)	10	0.25	347	100–555	17	0.86	0.92	46.7	3.4	1.0	6.6	69.7 ± 1.2	69.6			5.2	0.9			
	15	0.17	259	100–575	19	0.83	0.93	57.8	2.6	0.3	3.2	62.4 ± 0.8	61.8			3.1	2.0			
	18	0.22	449	100–575	19	0.82	0.94	108.9	2.8	1.5	2.4	63.6 ± 0.5	63.4				>ΔTRM			
	20	0.10	174	100–575	19	0.82	0.93	34.4	2.5	1.4	2.5	75.6 ± 1.7	74.7				>ΔTRM			
SBR-6038	02	0.50	611	100–460	9	0.48	0.86	22.9	3.6	3.6	5.7	76.1 ± 1.4	74.1	64.9 ± 5.7	62.8		>ΔTRM	62.7 ± 5.7	12.3	11.4
(1000–1057 AD)	03	0.74	1123	100–555	15	0.90	0.89	64.6	2.9	0.6	4.6	65.7 ± 0.8	63.9				>ΔTRM			
	06	1.95	3430	100–495	11	0.80	0.87	44.3	3.1	1.5	3.8	61.9 ± 1.0	59.4			-2.2	–1.1			
	07	0.52	1089	100–505	12	0.78	0.87	45.5	2.8	0.8	4.3	65.9 ± 1.0	65.8			0.8	0.0			
	10	1.65	2440	100–495	11	0.85	0.86	74.3	3.6	1.3	2.7	59.4 ± 0.6	60.3			2.3	2.3			
	13	1.22	2720	100–495	11	0.68	0.88	19.6	4.7	2.3	5.2	63.5 ± 1.9	64.4							
	15	3.10	3930	100–485	10	0.85	0.81	38.6	4.5	0.5	6.4	58.4 ± 1.0	57.0			1.2	0.9			
	16	1.30	2250	100–535	14	0.85	0.90	24.6	2.4	0.9	3.9	72.1 ± 2.2	70.4			1.1	1.1			
SBR-6043	01	0.56	1302	100–460	9	0.85	0.83	131.2	2.3	1.3	1.9	56.5 ± 0.3	58.7	60.2 ± 4.4	58.3		>ΔTRM	58.0 ± 4.5	11.3	10.6
(1000–1057 AD)	03	0.03	131	100–575	19	0.85	0.94	88.0	2.7	4.2	4.7	62.2 ± 0.6	62.9				>ΔTRM			
	07	0.34	900	100–460	9	0.68	0.86	70.6	3.2	3.2	3.7	59.5 ± 0.5	59.5							
	09	0.29	708	100–400	7	0.88	0.78	166.4	2.2	2.0	3.6	59.4 ± 0.2	59.5							
	10	0.86	1057	100–555	15	0.85	0.91	39.9	2.2	0.7	2.5	67.4 ± 1.3	65.8				>ΔTRM			
	13	0.96	1734	100–460	9	0.71	0.85	155.6	5.3	0.3	10.5	53.0 ± 0.2	53.8			2.4	1.3			
	15	0.03	110	100–575	16	0.79	0.92	20.7	3.7	4.4	5.5	66.1 ± 2.3	65.6			0.9	0..0			
	21	0.37	1126	100–460	9	0.80	0.84	97.4	2.3	3.3	5.1	55.8 ± 0.4	55.6							

Table 3. (*Continued.*)

Kiln	Sp.	NRM ($A\,m^{-1}$)	κ (10^{-6})	$T_{min}-T_{max}$ (°C)	n	f	g	q	MAD (°)	DANG (°)	CRM (per cent)	$F \pm \sigma F$ (μT)	F_e (μT)	Fm ± sd (μT)	Fpo (μT)	ΔTRM (24 hr) (per cent)	alt. (24 hr) (per cent)	Fpocr (μT)	VDM 10^{22} A m^2	VADM 10^{22} A m^2
SBR-6081	04	0.82	1257	100–430	8	0.91	0.72	43.3	2.3	1.0	2.7	65.0 ± 1.0	65.2	60.6 ± 3.3	59.6			58.6 ± 4.3	11.0	10.7
(1000–1057 AD)	06	1.32	2170	100–460	9	0.70	0.83	134.1	4.6	2.9	4.5	56.5 ± 0.3	55.3				> ΔTRM			
	08	1.83	2200	100–460	9	0.90	0.65	116.8	2.9	1.4	3.8	59.7 ± 0.3	58.9							
	11	0.06	246	100–460	9	0.71	0.87	41.3	4.0	2.0	5.7	62.0 ± 0.9	60.2			11.5	2.4			
	12	0.13	416	100–525	13	0.85	0.90	40.0	3.7	1.0	5.1	59.3 ± 1.1	59.1			6.6	5.1			
	13	0.09	312	100–460	9	0.62	0.86	45.1	4.7	0.8	3.6	59.2 ± 0.7	59.1			1.9	1.2			
	16	1.52	2320	100–460	9	0.86	0.73	72.2	3.2	0.9	2.9	63.7 ± 0.6	63.3							
	20	0.18	380	100–460	9	0.80	0.79	43.8	4.7	1.9	5.1	64.8 ± 0.9	64.0			3.3	–1.5			
RHA	02	1.41	2940	150–540	12	0.78	0.90	68.6	2.9	1.4	2.5	44.2 ± 0.5	45.9	47.2 ± 4.1	46.2	3.9	–1.9	45.7 ± 4.4	10.4	8.5
(1290–1410 AD)	05	1.51	1570	250–540	10	0.60	0.88	49.6	2.1	1.3	1.9	43.8 ± 0.5	44.0			2.5	–1.8			
	09	1.50	3896	100–480	11	0.83	0.90	75.4	1.8	0.5	2.2	47.1 ± 0.5	43.9				> ΔTRM			
	10	0.55	1570	300–540	9	0.65	0.85	14.0	5.8	4.1	1.6	52.5 ± 2.1	47.9				> ΔTRM			
	12	3.09	2030	150–540	12	0.75	0.89	44.5	3.6	1.8	4.3	57.3 ± 0.9	47.4				> ΔTRM			
	15	1.99	4060	200–540	11	0.73	0.87	27.4	3.9	2.3	4.8	60.9 ± 1.4	55.8				> ΔTRM			
	17	1.85	3526	250–540	10	0.54	0.88	53.5	1.8	2.4	3.0	45.9 ± 0.4	45.7				> ΔTRM			

agreement with the observed IRM unblocking temperatures (see Section 4). Only four specimens were rejected, three from kiln RHA and one from kiln SBR-FV. The criteria used to retain or reject archaeointensity determinations were the same as those described in Gómez-Paccard *et al*. (2006a). pTRM checks were considered positive if, at a given temperature step, the difference between the original pTRM and the pTRM check does not exceed 10 per cent of the total TRM acquired. The four rejected specimens failed to show a linear NRM-TRM plot or yielded unsuccessful pTRM checks (e.g. Figs 7g and h).

The quality of the obtained archaeointensity data has been assessed using the typical parameters of archaeointensity studies (e.g. Gómez-Paccard *et al*. 2006a) and are described in Table 3. The majority of the archaeointensity determinations have f factors bigger than 0.6 (Fig. 8a). One specimen with a f factors equal to 0.48 has also been accepted. All the specimens had MAD (Kirschvink 1980) values lower than 6° (Fig. 8b), and DANG (Pick & Tauxe 1993) values lower than 5° (Fig. 8c). The potential error of the archaeointensity caused by chemical remanent magnetization acquisition during Thellier experiments (the CRM parameter, Coe *et al.* 1984) was lower than 8 per cent for all the samples except SBR-6043–13, which had a value of 10.5 per cent (Table 3 and Fig. 8d). It is worth mentioning that a maximum acceptable CRM of 15 per cent has been retained by Gómez-Paccard *et al*. (2006a).

The effect of TRM anisotropy and cooling rate upon TRM intensity acquisition should be determined and field strength estimations for each specimen must be corrected appropriately (e.g. Chauvin *et al*. 2000; Genevey & Gallet 2002; Gómez-Paccard *et al*. 2006a, 2008). As expected for the kind of material analysed (burned clay or bricks from kilns, e.g. Kovacheva *et al.* 2009b) the effects of TRM anisotropy are generally low, and very similar values of the intensity before and after TRM anisotropy correction were obtained (Table 3 and Fig. 9a). In only two cases (RQD-105–02 and RHA-12) did the difference exceed 10 per cent.

The cooling rate dependence of TRM intensity was investigated for a cooling time of about 24 hr, assumed to be of the same order as the ancient cooling time of the structures, although there is no strong evidence to support this. In some cases, specimens broke during experiments and cooling rate correction factors could not be determined. As in previous studies, the cooling rate effect was quantified by carrying out supplementary TRM acquisition steps after the end of Thellier experiments. The archaeointensity values were corrected for specimens whose cooling rate correction factor was bigger than the magnetochemical alteration factor. This alteration factor quantifies the amount of magnetochemical changes that took place during the supplementary cycle of measurements (Gómez-Paccard *et al*. 2006a for further details). Fig. 9(b) shows the applied correction factors per specimen. A total of 22 archaeointensity values were corrected. In general, cooling rate correction factors were low (less than 4 per cent) and only two specimens showed correction factors higher than 10 per cent (12.6 per cent for SBR-FV-03 and 11.5 per cent for SBR-6081–11). Therefore, when cooling rate correction factors could not be determined the uncorrected archaeointensities were retained to calculate mean site intensities. The archaeointensity estimations per specimen presented in Table 3 fulfill the most demanding of quality criteria and are corrected for TRM anisotropy and cooling rate effects, where appropriate, so that the results can be considered of high quality.

Mean archaeointensities per kiln were calculated using between five and eight archeointensity values per structure and were derived considering the weighting factor of Prévot *et al.* (1985) for each specimen. The dispersion of the means was expressed as the

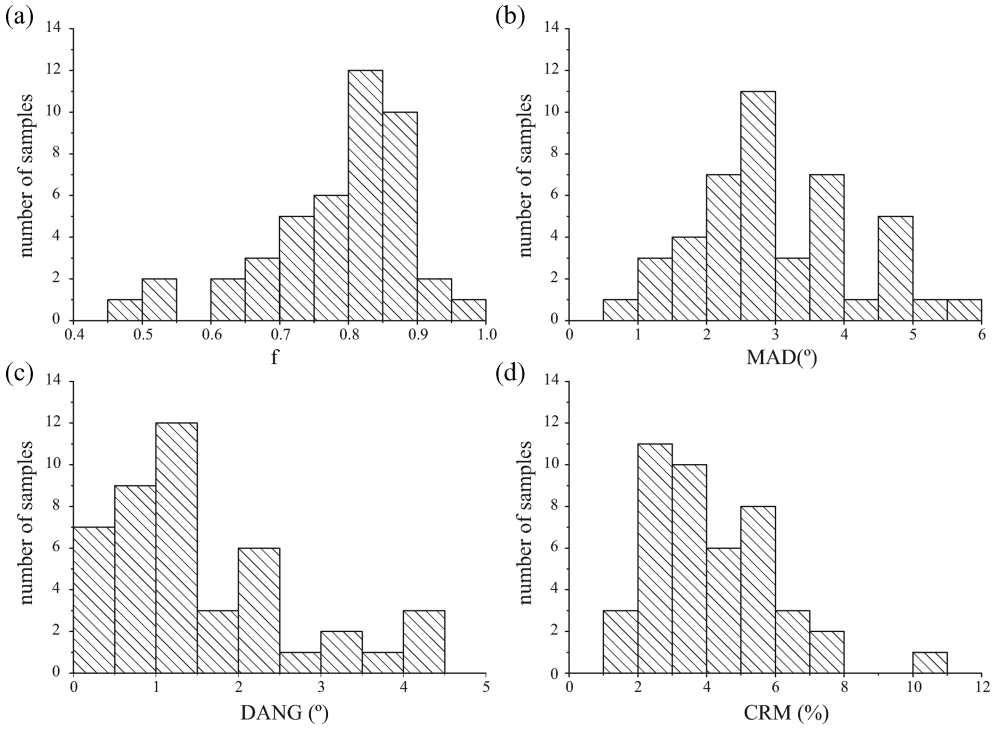

Figure 8. Variations of some parameters used to test the quality of archaeointensity determinations. (a) f, fraction of the NRM component used in the slope calculation; (b) MAD, maximum angular deviation; (c) DANG, deviation angle and (d) CRM, potential error on the estimation of the archaeointensity due to the acquisition of chemical remanent magnetization as a percentage of the applied field.

standard deviation (Table 3). Very small TRM anisotropy corrections were performed at a site level, with differences between the uncorrected and the TRM anisotropy corrected means less than 2 per cent for the five Tunisian kilns and 4.7 per cent for the Moroccan kiln (RHA). Differences between TRM anisotropy corrected and cooling rate and TRM anisotropy corrected intensity means are lower than 3 per cent for all of the studied kilns. For kilns SBR-FV, SBR-6038, SBR-6043 and SBR-6081 the differences between uncorrected and TRM anisotropy and cooling rate corrected mean intensities (Fpocr in Table 3) are less than 3 per cent. For kilns RQD-105 and RHA these differences are higher (4.4 and 5.8 per cent, respectively). These results highlight the need for TRM anisotropy and cooling rate corrections in archaeomagnetic studies if reliable mean archaeointensity estimates are to be obtained. Values of the standard deviation of 7–10 per cent of the estimated archaeointensities were obtained for all the kilns except SBR-FV, for which a value of 12.6 μT was obtained (20 per cent of the estimated archaeointensity, Table 3).

All four kilns from Sabra al-Mansuriya (SBR-FV, SBR-6038, SBR-6041 and SBR-6081) exhibited similar intensity values (see Table 3). This is consistent with the archaeological and stratigraphical constraints that suggest a similar age for the kilns. The lowest intensity value was observed for kiln RHA (Morocco, Table 3). The new results obtained for Morocco and Tunisia are plotted in Figs 10(a) and (b). The Tunisian results indicate that high intensities of about 66 μT occurred in this region during the 9th century AD (Fig. 10b). This result is in agreement with available European data that indicate that a rapid intensity fluctuation around 800 AD occurred in Europe (Genevey & Gallet 2002; Gallet *et al*. 2009; Kovacheva *et al*. 2009a). Although more data are clearly needed to confirm the occurrence of this fluctuation in North Africa it seems that it is also observed in this region.

6 DISCUSSION

6.1 Maghemite and archaeointensity results

Rock magnetic results suggest that the magnetic properties of the studied baked clays are in most cases dominated by magnetite, titanomagnetite (with variable but generally low Ti content) and maghemite. Each one of these magnetic phases contributed to the stable NRM retained by the burned clays. As expected for this kind of material the archaeomagnetic experiments carried out were successful for the majority of the samples analysed. Therefore the maghemite identified during rock-magnetic experiments (Section 4) shows a high degree of thermal stability, something that has been observed in synthetic (Özdemir & Banerjee 1984) and natural material (e.g. Gehring *et al*. 2009), including archaeomagnetic material (Jordanova *et al*. 1997).

It is the origin of stable maghemite that is of importance in archaeointensity studies and whether it carries a natural remanence that is chemical or thermal in nature. Stable maghemite formed through low-temperature oxidation (of magnetite, for instance) may acquire a chemical remanence (CRM). If it subsequently acquires a TRM during the intensity experiments then this would lead to a bias on the past field intensity determination.

Alternatively, maghemite may form through high-temperature processes, for example, the transformation of lepidocrocite during heating (Gendler *et al*. 2005). This study showed that the newly formed stable maghemite could acquire a TRM after multiple heating, giving rise to linear Arai plots until it starts to transform to hematite at temperatures above 550°C. Therefore thermally stable maghemite may also carry a thermoremanent NRM component and may behave ideally in archaeointensity experiments—with the limitations and caveats that normally apply to such experiments. Indeed,

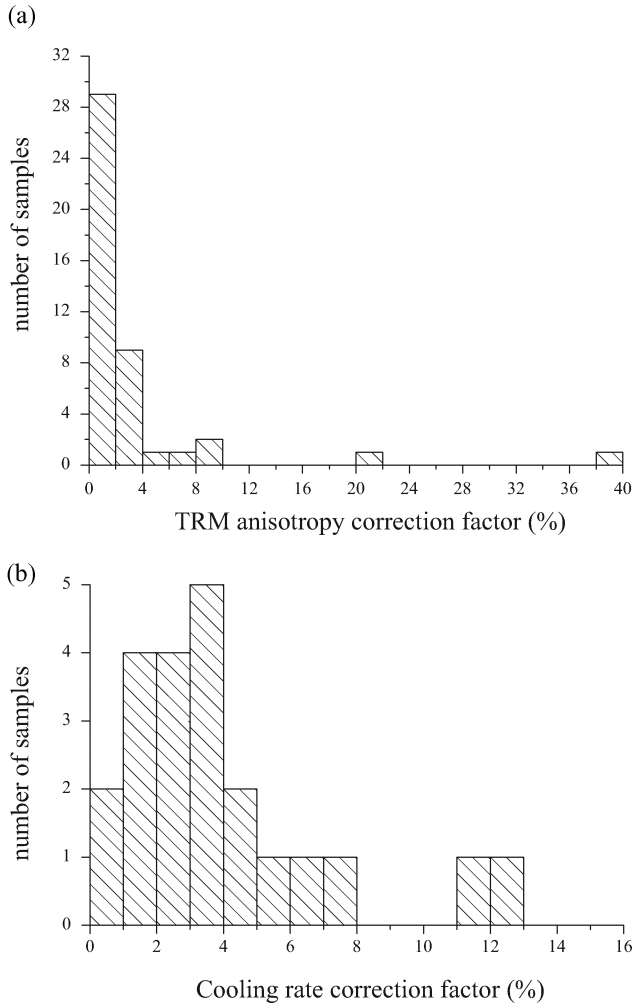

Figure 9. Correction factors per specimen applied to take into account the effect of (a) TRM anisotropy and (b) cooling rate upon archaeointensity. A cooling time of about 24 hr has been used to calculate the cooling rate correction factors.

this was found to be the case by Schnepp *et al.* (2009) in magnetite and maghemite bearing oven floors.

In this scenario the limiting factor may be the temperature reached by the burned clays. In the Gendler *et al*. (2005) study, the maghemites began to transform beyond 550°C, whereas the maghemites of Jordanova *et al*. (1997) and Gehring *et al.* (2009) were stable beyond their Curie temperatures of around 650°C. The temperatures reached by burned clays (and subsequently their magnetic properties) depend on their position with respect the heat source and their thermal properties. Some parts of the kiln may then reach temperatures that do not exceed 600°C (Spassov & Hus 2006) and so the clays might then be expected to retain any stable maghemite that may have formed.

In the context of this study, the distribution of maghemite-bearing samples with respect to their location within each block sample is poorly constrained, so that determining their relation with respect to the combustion chamber is not possible. Furthermore their position with respect to the external part of the kiln structure is not constrained, which might have some bearing on the degree to which they may have suffered post-abandonment low temperature oxidation. This information should be recorded in future studies that may then address the question of the origin of stable maghemite in archaeomagnetic material.

6.2 Comparison with other available archaeomagnetic data

The new archaeomagnetic data obtained have been compared with other available data from neighbouring regions by compiling the archaeomagnetic data available for the last two millennia from Europe and North Africa. Historical volcanic Italian data have not been included due to the often present dating uncertainties and/or difficulties identifying with certainty the eruptive products from specific volcanic events (e.g. Tanguy *et al*. 2003; Tema *et al*. 2006). The archaeomagnetic compilations of Donadini *et al*. (2009) and Genevey *et al*. (2008) have been supplied with recent data (Ben-Yosef *et al.* 2008; Casas *et al.* 2008; Catanzariti *et al.* 2008; De Marco *et al.* 2008; Donadini *et al.* 2008, 2010; Gómez-Paccard *et al*. 2008; Herries *et al.* 2008; Peters *et al.* 2008; Ruiz-Martinez *et al.* 2008; Sapin *et al.* 2008; Suteu *et al.* 2008; Tema & Lanza 2008; Gallet *et al*. 2009; Genevey *et al.* 2009; Hartmann *et al*. 2009; Kovacheva *et al.* 2009a; Márton 2009, 2010; Nachasova & Burakov 2009; Schnepp *et al*. 2009; Tema *et al*. 2010). The location of the archaeomagnetic sites is plotted in Fig. 1. Only seven directional data (Kovacheva 1984; Najid 1986) and four archaeointensity values (Kovacheva 1984; Casas *et al*. 2008) have been published for Morocco. For Tunisia no archaeomagnetic data are available for the last 2000 years but one intensity data from Libya close to the Tunisian border is included in the study of Odah *et al.* (1995).

Two reference locations (Rirha in Morocco and Sabra al-Mansuriya in Tunisia) and two restricted regions of 800 km of radius centred at both locations have been defined (Fig. 1). The western selected area contains archaeomagnetic data from the Iberian Peninsula (described in Gómez-Paccard *et al*. 2006c, 2008) and the available Moroccan data obtained close to the Rirha archaeological site (Supporting Information). For the region centred at Sabra al-Mansuriya, all data come from Italy (see the compilations of Tema *et al*. 2006, 2010) except the one located at Libya (Odah *et al*. 1995). Directional and intensity data have been relocated to the corresponding reference location via the virtual geomagnetic pole and the virtual dipole moment (VDM), respectively (Fig. 10). The new data (directions and intensity) obtained for Morocco are in good agreement with the compiled data selected for the Rirha region (Fig. 10a, and Supporting Information). For the Sabra al-Mansuriya region no directional or intensity data are available covering the intervals of interest of this study (Fig. 10b).

6.3 Comparison with regional and global geomagnetic field models

The new data obtained can be compared with global and regional models of the Earth's magnetic field. For comparison the global model ARCH3k.1 has been used. This model belongs to the last series of the Continuous Archaeomagnetic Lake Sediment family of models (Korte *et al.* 2009) developed using the spherical harmonic analysis. The ARCH3k.1 model is based on a global compilation of archaeomagnetic and volcanic data distributed all around the world (Donadini *et al.* 2009). These models represent the palaeofield at a global scale, but they are usually too smooth to represent rapid changes of the Earth's magnetic field (Pavón-Carrasco *et al.* 2009).

An intermediate approach between local PSV curves (not available for Morocco and Tunisia) and global geomagnetic models is the

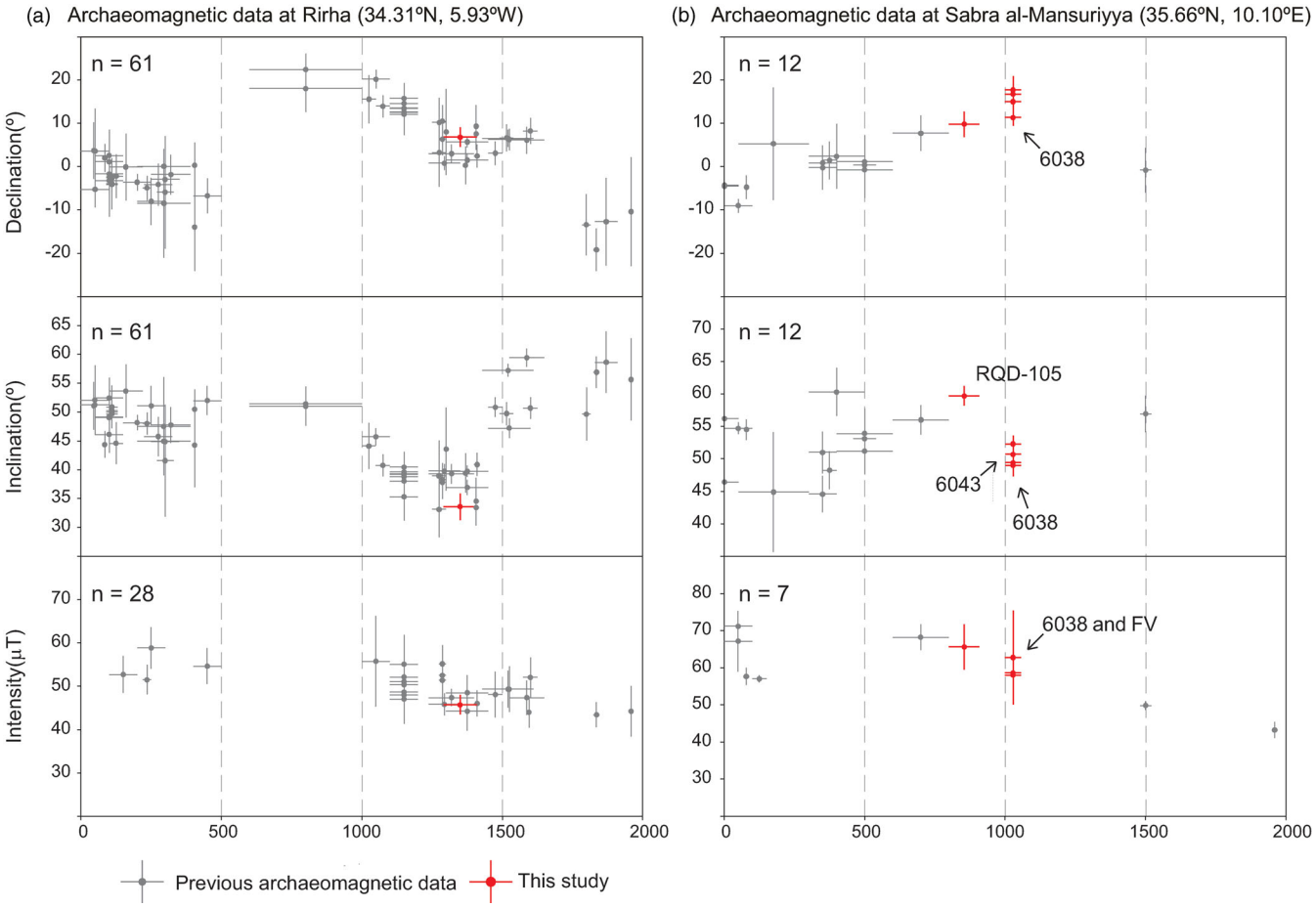

Figure 10. Comparison of the data obtained in this study (in red) with previous data (in grey) from locations less than 800 km from the studied sites (Fig. 1). The value of *n*, the number of previous data available, is indicated.

determination of regional models. Recently a new regional spherical cap harmonic model has been developed (Pavón-Carrasco *et al.* 2009). This SCHA.DIF.3k model is based on archaeomagnetic data (volcanic data are not included) from the European continent and neighbouring areas and is valid for Europe, North Africa and western Asia. These approaches (SCHA.DIF.3k and ARCH3k.1 models) may be the best possible solution to describe the long-term geomagnetic variations in Northwest Africa.

The results derived from the global (ARCH3k.1) and regional (SCHA.DIF.3k) geomagnetic field models are represented in Fig. 11 at Rirha and Sabra al-Mansuriya coordinates. Both the regional and global models predict similar variation of the Earth's magnetic field at both locations. The models fit reasonably well the directional data available for the Rirha (Fig. 11a) and Sabra al-Mansuriya (Fig. 11b) regions, taking into account the dispersion observed.

It is worth mentioning the large inclination difference (more than 20°) between the data obtained by Márton *et al*. (1992) for the beginning of the fifth century AD and other data and model results available for this period (Fig. 10b and Supporting Information). The mean archaeomagnetic direction obtained by Márton *et al*. (1992) is very similar to the one obtained from the same archaeological structure and reported by Evans & Hoye (2005), which is in fact a revised version of a previous study (Evans & Mareschal 1987). This supports the reliability of the palaeomagnetic direction published by Márton *et al*. (1992). However, the anomalous high inclination and the large age uncertainty reported for this structure indicate that the mean age ascribed might be not well constrained. Archaeomagnetic results suggest that this structure is probably younger than the mean age proposed.

It should also be highlighted that these two (or even three) archaeomagnetic results corresponding to the same archaeological structure are reported separately in the available databases (Tema *et al*. 2006; Donadini *et al*. 2009). As it is really difficult to control all the available archaeomagnetic data, future publications including a revision of older studies must state clearly the archaeomagnetic data that have been updated. Data repetition and dating inaccuracies must be avoided when constructing regional SV curves or geomagnetic field models if accurate estimations of geomagnetic field changes are to be obtained.

Considering the complete archaeointensity data set it seems that geomagnetic field models underestimate intensity values at Rirha coordinates between the 11th and 17th centuries AD (Figs 10a and 11a). All the archaeointensity data selected for this region have been obtained from Thellier or Thellier derived methods, except the one obtained by Casas *et al.* (2008) which was obtained by microwave experiments, and generally are based on more than six samples per site (Supporting Information). Therefore they can be considered highly reliable. The majority of the archaeointensity compiled for this region are not included in the construction of the regional SCHA.DIF.3k or global ARCH3k.1 models. Therefore the recently obtained Spanish archaeointensities (Gómez-Paccard *et al*. 2008) as well as the new African data obtained here will improve the

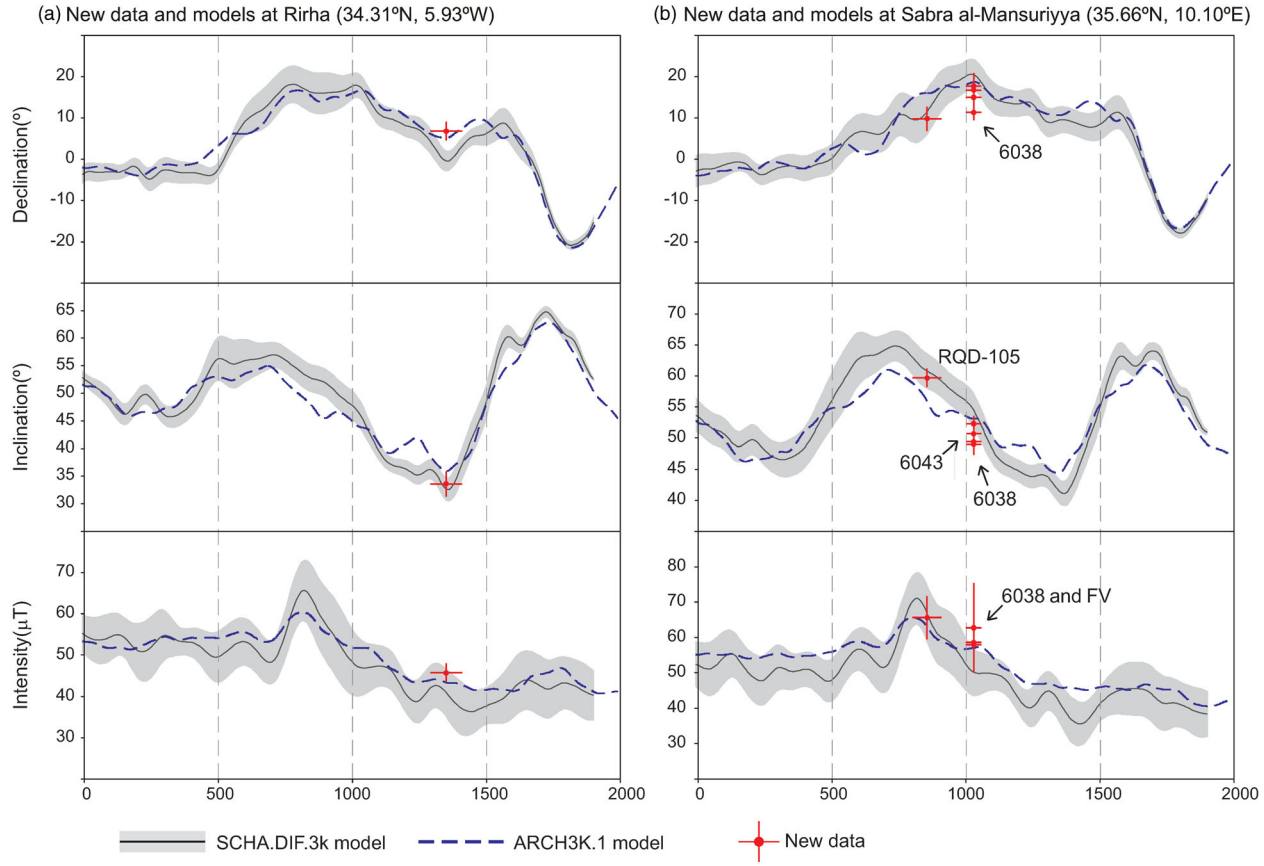

Figure 11. Comparison of the data obtained in this study (in red) with geomagnetic field models results. Values predicted by the regional SCHA.DIF.3 (Pavón-Carrasco *et al.* 2009) and global ARCH3k.1 (Korte *et al*. 2009) are showed in grey and blue, respectively.

accuracy of future geomagnetic field models in Northwest Africa and Southwest Europe.

For the Sabra al-Mansuriya region the models results fit reasonably well the new archaeointensity data obtained (Fig. 11b). The low number of previous intensity data for this region prevents a reliable comparison for the overall period. However, it can be seen that some of the archaeointensity data obtained by the Shaw technique (Evans 1986) gives 'anomalous' high intensities for the 1st century AD (Figs 10b and 11b). This high intensity period is not observed in the more numerous south European data. Some of these data are also based on a very low number of independent samples (one or two) (Supporting Information). Chauvin *et al.* (2000) mention that the validity of some of the published intensity data is often disputable. Therefore, these high intensities values for the 1st century AD might not be reliable. More data are needed to infer a robust description of geomagnetic field intensity changes in Tunisia.

Finally, it should be noted that predictions of geomagnetic field models in Northwest Africa could be affected by the low number of data available for this region—especially archaeointensity data. However, some discrepancies may also be due to the fact that geomagnetic models use all of the archaeointensity data available without a pre-selection process based on their quality. Overall the results highlight the need to obtain more reliable data for North Africa, such as the new data presented here.

7 CONCLUSIONS

An archaeomagnetic study of archaeological kilns from Tunisia and Morocco yielded six well-defined site-mean characteristic remanence directions of magnetization and six new robust and highly reliable archaeointensity data, corrected for both the effect of TRM anisotropy and cooling rate upon TRM intensity acquisition. The results showed that TRM anisotropy and cooling rate corrections are significant in the determination of the mean site intensities in two of the six structures studied, with differences of 4.4 and 5.8 per cent between uncorrected and corrected mean intensities indicating that these corrections must be investigated when studying archeomagnetic materials if accurate archaeointensity determinations are to be obtained.

Rock magnetic analysis showed that the principal magnetic carriers are magnetite and low Ti titanomagnetite, along with thermally stable maghemite and a high coercivity phase with low unblocking temperature. Both this high coercivity phase and the thermally stable maghemite contribute to the characteristic magnetization of the kilns and behave ideally during archaeointensity experiments.

The comparison between the new data obtained, previously available data from nearby regions and geomagnetic field models results (Korte *et al.* 2009; Pavón-Carrasco *et al.* 2009) show a general broad agreement. However, some differences are observed between intensity data and models results for the Moroccan region. The results also suggest that high intensities of about 65 μT occurred in Tunisia during the 9th century, in agreement with European archaeomagnetic data that indicate that a rapid intensity fluctuation occurred in Europe around 800 AD. The results highlight the need to obtain more data for North Africa if a reference SV curve valid for this region wants to be obtained, such as the new data obtained here. They are also suggestive of the requirement of performing

an archaeomagnetic data pre-selection based on quality criteria before modelling the geomagnetic field or before constructing PSV references curves.

ACKNOWLEDGMENTS

We would like to express our considerable thanks to Patrice Cressier and Mourad Rammah, from the Université Lumière-Lyon 2 (UMR 5648-CNRS) and the Institute National du Patrimoine (Tunisia), respectively, in allowing us to study the archaeological kilns from Sabra al-Mansuriya and Kairouan. We would like also to thank Laurent Callegarin and Mohamed Kbriri-Alaoui from the Université de Pau et des Pays de l'Adour and the Institut National des Sciences de l'Archéologie et du Patrimoine (Morocco), respectively, for providing us the opportunity to study the Rirha kiln. Their considerable interest and support on this project made possible this research. The thoughtful contributions of the two referees were also greatly appreciated. Financial support to this research was given by a CSIC JAE-Doc postdoctoral research contract (MGP), the Spanish Ministry of Education and Science (projects: CGL2008–02203/BTE, CGL2011–24790 and CGL2010-15767/BTE) and Banco Santander—Universidad Complutense de Madrid (Grupo de Investigación 910396).

REFERENCES

Ben-Yosef, E., Ron, H., Tauxe, L., Agnon, A., Genevey, A., Levy, T.E. & Avner, U., 2008. Application of copper slag in archeointensity research, *J. geophys. Res.,* **113**(B8), B08101, doi:10.1029/2007JB005235.

Callegarin, L., Kbiri-Alaoui, M., Ichkhakh, A., Darles, C. & Ropiot, V., 2006. Les opérations archéologiques maroco-françaises de 2004 et 2005 à Rirha (Sidi Slimane, Maroc), *Mélanges de la Casa de Velázquez,* **36**(2), 345–357.

Callegarin, L., Kbiri Alaoui, M., Ichkhakh, A. & Roux, J.-Cl., 2011. Le site antique et médiéval de Rirha (Sidi Slimane, Maroc), *Les Nouvelles de l'Archéologie,* **124,** 25–29.

Casas, L., Brianso, J.L., Alvarez, A., Benzzi, K. & Shaw, J., 2008. Archaeomagnetic intensity data from the Saadien Tombs (Marrakech, Morocco), late 16th century, *Phys. Chem. Earth,* **33,** 474–480.

Catanzariti, G., McIntosh, G., Gómez-Paccard, M., Ruiz-Martínez, V.C., Osete, M.L., Chauvin, A. & the AARCH Scientific Team, 2008. Quality control of archaeomagnetic determination using a modern kiln with a complex NRM, *Phys. Chem. Earth,* **33,** 427–437.

Chauvin, A., Garcia, Y., Lanos, P. & Laubenheimer, F., 2000. Paleointensity of the geomagnetic field recovered on archaeomagnetic sites from France, *Phys. Earth planet. Inter.,* **120**(1–2), 111–136, doi:10.1016/S0031-9201(00)00148-5.

Coe, R.S., Gromme, S. & Mankinen, E.A., 1984. Geomagnetic paleointensities from excursion sequences in lavas on Oahu, Hawaii, *J. geophys. Res,* **89,** 1059–1069.

Coll-Conesa, J., Callegarin, L., Thiriot, J., Fili, A., Kbiri-Alaoui, M. & Ichkhakh, A., 2011. Première approche de l'implantation islamique à Rirha (Sidi Slimane), *Bull. d'Arch. Maroc.,* **22**, in press.

Cressier, P. & Rammah, M., 2004. Une autre ville califale: Sabra al-Mansûriya, *Cuadernos de Madînat al-Zahrâ',* **5,** 241–255.

Cressier, P. & Rammah, M., 2006. Sabra al-Mansûriya (Kairouan, Tunisie): résultats préliminaires des datations par radio carbone, *Mélanges de l'École française de Rome. Moyen Âge,* **118**(2), 395–400.

Dassi, L., Zouari, K. & Faye, S., 2005. Identifying sources of groundwater recharge in the Merguellil basin (Tunisia) using isotopic methods: implication of dam reservoir water accounting, *Environ. Geol.,* **49,** 114–123.

Day, R., Fuller, M.D. & Schmidt, V.A., 1977. Hysteresis properties of titanomagnetites: grain size and composition dependence, *Phys. Earth planet. Inter.,* **13,** 260–267.

De Marco, E., Spatharas, V., Gomez-Paccard, M., Chauvin, A. & Kondopoulou, D., 2008. New archaeointensity results from archaeological sites and variation of the geomagnetic field intensity for the last 7 millennia in Greece, *Phys. Chem. Earth,* **33,** 578–595.

Donadini, F., Kovacheva, M., Kostadinova, M., Hedley, I.G. & Pesonen, L.J., 2008. Palaeointensity determination on an early medieval kiln from Switzerland and the effect of cooling rate, *Phys. Chem. Earth,* **33,** 449–457.

Donadini, F., Korte, M. & Constable, C.G., 2009. Geomagnetic field for 0–3 ka: 1. New data sets for global modeling, *Geochem. Geophys. Geosyst.,* **10**(6), Q06007, doi:10.1029/2008GC002295.

Donadini, F., Kovacheva, M. & Kostadinova, M., 2010. Archaeomagnetic study of ancient Roman lime kilns (1c. AD) and one pottery kiln (1c. BC – 1c. AD) at Krivina, Bulgaria, as a contribution to archeomagnetic dating, *Archeologia Bulgarica,* **XIV**(2), 213–225.

Evans, M.E., 1986. Paleointensity estimates from Italian kilns, *J. Geomag. Geoelector.,* **38,** 1259–1267.

Evans, M.E. & Hoye, G.S., 2005. Archaeomagnetic results from southern Italy and their bearing on geomagnetic secular variation, *Phys. Earth planet. Inter.,* **151,** 155–162.

Evans, M.E. & Mareschal, M., 1987. Secular variation and magnetic dating of fired structures in southern Italy, in *Proceedings of the 25th International Symposium in Archaeometry,* ed. Maniatis Y., Elsevier, Amsterdam.

Fisher, R.A., 1953. Dispersion on a sphere, *Proc. R. Soc.* **217,** 295–305.

Gallet, Y., Genevey, A., Le Goff, M., Warmé, N., Gran-Aymerich, J. & Lefèvre, A., 2009. On the use of archeology in geomagnetism, and vice-versa: recent developments in archeomagnetism, *C. R. Phys.,* **10**(7), 630–648.

Gehring, A.U., Fischer, H., Louvel, M., Kunze, K. & Weidler, P.G., 2009. High temperature stability of natural maghemite: a magnetic and spectroscopic study, *Geophys. J. Int.,* **179,** 1361–1371.

Gendler, T.S., Shcherbakov, V.P., Dekkers, M.J., Gapeev, A.K., Gribov, S.K. & McClelland, E., 2005. The lepidocrocite-maghemite-haematite reaction chain—I. Acquisition of chemical remanent magnetisation by maghemite, its magnetic properties and thermal stability, *Geophys J. Int.,* **160,** 815–832.

Genevey, A. & Gallet, Y., 2002. Intensity of the geomagnetic field in western Europe over the past 2000 years: new data from ancient French pottery, *J. geophys. Res.,* **107**(B11), 2285, doi:10.1029/2001JB000701.

Genevey, A., Gallet, Y., Constable, C.G., Korte, M. & Hulot, G., 2008. ArcheoInt: an upgraded compilation of geomagnetic field intensity data for the past ten millennia and its application to the recovery of the past dipole moment, *Geochem. Geophys. Geosyst.,* **9**(4), Q04038, doi:10.1029/2007GC001881.

Genevey, A., Gallet, Y., Rosen, J. & Le Goff, M., 2009. Evidence for rapid geomagnetic field intensity variations in Western Europe over the past 800 years from new French archeointenisity data, *Earth planet. Sci. Lett.*, **284,** 132–143.

Gómez-Paccard, M., Chauvin, A., Lanos, P., Thiriot, J. & Jiménez-Castillo, P., 2006a. Archeomagnetic study of seven contemporaneous kilns from Murcia (Spain), *Phys. Earth planet. Inter.,* **157**(1–2), 16–32, doi:10.1016/j.pepi.2006.03.001.

Gómez-Paccard, M., Chauvin, A., Lanos, P., McIntosh, G., Osete, M.L., Catanzariti, G., Ruiz-Martínez, V.C. & Núñez, J.I., 2006b. First archaeomagnetic secular variation curve for the Iberian Peninsula: comparison with other data from western Europe and with global geomagnetic field models, *Geochem. Geophys. Geosyst.,* **7,** Q12001, doi:10.1029/2006GC001476.

Gómez-Paccard, M. *et al*. 2006c. A catalogue of Spanish archaeomagnetic data, *Geophys. J. Int.,* **166,** 1125–1143, doi:10.1111/j.1365-246X.2006.03020.x.

Gómez-Paccard, M., Chauvin, A., Lanos, P. & Thiriot, J., 2008. New archeointensity data from Spain and the geomagnetic dipole moment in western Europe over the past 2000 years, *J. geophys. Res.,* **113**(B9), B09103, doi:10.1029/2008JB005582.

Hartmann, G.A., Trindade, R.I.F., Goguitchaichvili, A., Etchevarne, C., Morales, J. & Afonso, M.C., 2009. First archeointensity results from

Portuguese potteries (1550–1750 AD), *Earth Planets Space,* **61**(1), 93–100.

Herries, A.I.R., Kovacheva, M. & Kostadinova, M., 2008. Mineral magnetism and archaeomagnetic dating of a mediaeval oven from Zlatna Livada, Bulgaria, *Phys. Chem. Earth,* **33**(6–7), 496–510.

Iassanov, P.G., Nurgaliev, D.K., Burov, D.V. & Heller, F., 1998. A modernized coercivity spectrometer, *Geologica Carpathica,* **49**(3), 224–226.

Jordanova, N., Petrovsky, E. & Kovacheva, M., 1997. Preliminary rock magnetic study of archeomagnetic samples from Bulgarian prehistoric sites, *J. Geomagn. Geoelectr.,* **49,** 543–566.

Kirschvink, J.L., 1980. The least-squares line and plane and the analysis of paleomagnetic data, *Geophys. J. R. astron. Soc.,* **62,** 699–718.

Korte, M., Donadini, F. & Constable, C.G., 2009. Geomagnetic field for 0–3 ka: 2. A new series of time-varying global models, *Geochem. Geophys. Geosyst.,* **10**(6), Q06008, doi:10.1029/2008GC002297.

Kovacheva, M., 1984. Some archaeomagnetic conclusions from three archaeological localities in north-west Africa, *C. R. Acad. Sci. Bulgaria,* **37,** 171–174.

Kovacheva, M., Boyadziev, Y., Kostadinova-Avramova, M., Jordanova, N. & Donadini, F., 2009a. Updated archeomagnetic data set of the past 8 millennia from the Sofia laboratory, Bulgaria, *Geochem., Geophys., Geosyst.,* **10,** Q05002, doi:10.1029/2008GC002347.

Kovacheva, M., Chauvin, A., Jordanova, N., Lanos, P. & Karloukovski, V., 2009b. Remanence anisotropy effect on the palaeointensity results obtained from various archaeological materials, excluding pottery, *Earth Planets Space,* **61,** 711–732.

Lowrie, W., 1990. Identification of ferromagnetic minerals in a rock by coercivity and unblocking temperature properties. *Geophys. Res. Lett.* **17,** 159–162.

Márton, P., 2009. Prehistorical archaeomagnetic directions from Hungary in comparison with those from south-eastern Europe, *Earth Planets Space,* **61**(12), 1351–1356.

Márton, P., 2010. Two thousand years of geomagnetic field direction over central Europe revealed by indirect measurements, *Geophys. J. Int.,* **181**(1), 261–268.

Márton, P., Abdeldayem, D., Tarling, D.H., Nardi, G. & Pierattini, D., 1992. Archaeomagnetic study of two kilns at Segesta, Sicily, *Sci. Tech. Cultural Heritage,* **I,** 123–127.

Maury, R.C. *et al*., 2000. Post-collisional Neogene magmatism of the Mediterranean Maghreb margin: a consequence of slab breakoff, *C. R. Acad. Sci. Ser. IIa Sci Terre Planetes,* **331,** 159–173.

McIntosh, G., Kovacheva, M., Catanzariti, G., Osete, M.L. & Casas, L., 2007. Widespread occurrence of a novel high coercivity, thermally stable, low unblocking temperature magnetic phase in heated archeological material, *Geophys. Res. Lett.,* **34,** L21302, doi:10.1029/2007GL031168.

McIntosh, G., Kovacheva, M., Catanzariti, G., Donadini, F. & Osete, M.L., 2011. High coercivity remanence in baked clay materials used in archeomagnetism, *Geochem. Geophys. Geosyst.,* **12,** Q02003, doi:10.1029/10.1029/2010GC003310.

Nachasova, I.E. & Burakov, K.S., 2009. Variation of the intensity of the Earth's magnetic field in Portugal in the 1st millenium BC, *Phys. Solid Earth,* **45,** 54–62.

Najid, D., 1986. Palaeomagnetic studies in Morocco, *PhD thesis,*. University of Newcastle upon Tyne.

Odah, H., Heider, F., Hussain, A.G., Hoffmann, V., Soffel, H. & Elgamili, M., 1995. Paleointensity of the geomagnetic field in Egypt from 4000BC to 150AD using the Thellier method, *J. Geomagn. Geoelectr.,* **47**(1), 41–58.

Özdemir, Ö. & Banerjee, S.K., 1984. High temperature stability of maghemite (γ-Fe_2O_3), *Geophys. Res. Lett.,* **11,** 161–164, doi:101.1029/GL011i003p00161.

Pavón-Carrasco, F.J., Osete, M.L., Torta, J.M. & Gaya-Piqué, L.R., 2009. A regional archeomagnetic model for Europe for the last 3000 years, SCHA.DIF.3K: Applications to archeomagnetic dating, *Geochem. Geophys. Geosyst,* **10**(3), Q03013, doi:10.1029/2008GC002244.

Peters, C., Abrahamsen, N., Voss, O., Batt, C.M. & McDonnell, G., 2008. Magnetic investigations of iron age slags at Yderik, Denmark: mineral magnetic comparison to UK slags, *Phys. Chem. Earth,* **33**(6–7), 465–473.

Pick, T. & Tauxe, L., 1993. Holocene paleointensities: thellier experiments on submarine basaltic glass from the East Pacific Rise, *J. geophys. Res.,* **98**(B10), 17 949–17 964.

Prévot, M., Mankinen, E.A., Coe, R.S. & Gromé, C.S., 1985. The Steens Mountain (Oregon) geomagnetic polarity transition. 2. Field intensity variations and discussion of reversal models, *J. geophys. Res.,* **90,** 10 417–10 448.

Ruiz-Martinez, V.C., Pavon-Carrasco, F.J. & Catanzariti, G., 2008. First archaeomagnetic data from northern Iberia, *Phys. Chem. Earth,* **33**(6–7), 566–577.

Sapin, C., Baylé, M., Büttner, S., Guibert, P. & Blain, S., 2008. Archéologie du bâti et archéométrie au Mont-Saint-Michel, nouvelles approches de Notre-Dame-Sous-Terre, *Archéologie Médiévale,* **38,** 71–122.

Schnepp, E. & Lanos, P., 2005. Archaeomagnetic secular variation in Germany during the past 2500 years, *Geophys. J. Int.,* **163,** 479–490.

Schnepp, E., Lanos, P. & Chauvin, A., 2009. Geomagnetic paleointensity between 1300 and 1750 AD derived from a bread oven floor sequence in Lubeck, Germany, *Geochem. Geophys. Geosyst.,* **10**(8), Q08003, doi:10.1029/2009GC002470.

Spassov, S. & Hus, J., 2006. Estimating baking temperatures in a Roman pottery kiln by rock magnetic properties: implications of thermochemical alteration on archaeointensity determinations, *Geophys. J. Int.,* **167,** 592–604.

Suteu, C.A., Batt, C.M. & Zananiri, I., 2008. New developments in archaeomagnetic dating for Romania—A progress report on recent directional studies, *Phys. Chem. Earth,* **33**(6–7), 557–565.

Tanguy, J.C., Le Goff, M., Príncipe, C., Arrighi, S., Chillemi, V., Paiotti, A., La Delfa, S. & Patanè, G., 2003. Archaeomagnetic dating of Mediterranean volcanics of the last 2100 years: validity and limits, *Earth planet Sci. Lett.,* **211,** 111–124.

Tauxe, L., 1998. Modern approaches in geophysics, in *Paleomagnetic Principles and Practice,* Vol. 17, Kluwer Academic, Dordrecht.

Tema, E., Hedley, I. & Lanos, P., 2006. Archaeomagnetism in Italy: a compilation of data including new results and a preliminary Italy secular variation curve, *Geophys. J. Int.,* **167**(3), 1160–1171, doi:10.1111/j.1365-246X.2006.03150.x.

Tema, E. & Lanza, R., 2008. Archaeomagnetic study of a lime kiln at Bazzano (northern Italy), *Phys. Chem. Earth,* **33**(6–7), 534–543.

Tema, E., Goguitchaichvili, A. & Camps, P., 2010. Archaeointensity determinations from Italy: new data and the Earth's magnetic field strength variation over the past three millennia, *Geophys. J. Int.,* **180**(2), 596–608.

Thellier, E. & Thellier, O., 1959. Sur l'intensité du champ magnétique terrestre dans le passé historique et géologique, *Ann. Géophys.,* **15,** 285–376.

Thiriot, J., 2009. Les structures de cuisson de l'atelier de potiers du "palais" de Sabra al-Mansûriya (Kairouan, Tunisie), in *Actas del VIII Congreso Internacional de Cerámica Medieval en el Mediterráneo.,* Vol. 2, pp. 685–695, eds Zozaya, J., Retuerce, M., Hervás, M.Á. & De Juan, A., Ciudad Real, 2006 February 27–March 3.

SUPPORTING INFORMATION

Additional Supporting Information may be found in the online version of this article:

Table S1. Archaeomagnetic directional data for the last two millennia compiled within a restricted region of 800 km of radius around Rirha.

Table S2. Archaeointensity data for the last two millennia compiled within a restricted region of 800 km of radius around Rirha.
Table S3. Archaeomagnetic directional data for the last two millennia compiled within a restricted region of 800 km of radius around Sabra al-Mannsuriya.
Table S4. Archaeointensity data for the last two millennia compiled within a restricted region of 800 km of radius around Sabra al-Mansuriya.

Please note: Wiley-Blackwell are not responsible for the content or functionality of any supporting materials supplied by the authors. Any queries (other than missing material) should be directed to the corresponding author for the article.